Solid Freeform Fabrication 2024: Proceedings of the 35th Annual International Solid Freeform Fabrication Symposium – An Additive Manufacturing Conference
Reviewed Paper

TOWARDS AFFORDABLE ALUMINUM ADDITIVE MANUFACTURING: CONSIDERATIONS ON THE MANUFACTURING OF NON-EXPLOSIBLE NExP-1 ALSi10Mg ON MEDIUM-WATTAGE SYSTEMS

F. N. Depboylu*, A. A Popa*, T. Oyama†, Y. Ono†

* Department of Mechanical and Electrical Engineering (DME) and Mechatronics (Center of Industrial Mechanics), University of Southern Denmark, DK-6400, Sønderborg, Denmark
†Additive Manufacturing Innovation Center, Taiyo Nippon Sanso Corporation, 142-8558, Tokyo, Japan

Abstract

Laser powder bed fusion of aluminum poses safety challenges due to the reactive nature of the feedstock. The non-explosible claim of the NExP-1 AlSi10Mg from Equispheres has been validated through Lower Explosive Limit and Minimum Ignition Energy, ranking it in the lowest explosion class per JIS Z 8817. This relieves the need for otherwise costly investment in the manufacturing environment. With its enhanced flowability and homogenously spherical particles above 100 µm in average size distribution, the feedstock facilitates faster build rates at high layer thickness. Attempting to utilize this powder on a 400 W Yb laser, well below the 700 W for which it was designed, leads to atypical energy behavior within the melt pool. The necessary process parameter development was analyzed with density and mechanical characteristics highlighting the promising future of affordable aluminum additive manufacturing for lightweight applications.

Key Words: Laser Powder Bed Fusion, Aluminum, Explosibility, Mechanical Features

Introduction

AlSi10Mg has become a preferred alloy in microelectronic applications that require high electrical and thermal conductivities within lightweight structures [1,2,3]. Laser-powder bed fusion technology (L-PBF) contributes to the popularity of AlSi10Mg by enabling the manufacturing of intricate geometries (such as lattices) for lightweight applications with increased surface area [3,4]. Moreover, the presence of silicon (Si) in the alloy accelerates solidification by lowering the melting point. It improves weldability by reducing the penetrating energy to melt the powder while Mg formation within β´´ increases mechanical strength by Mg_2Si precipitation [5]. The benefits of Si and Mg render AlSi10Mg a suitable feedstock for L-PBF. However, aluminum powder, with its fine particle size characteristics of below 420 µm, is on the Special Health Hazardous Substance list due to being prone to flammability and high affinity for oxidation [3]. Furthermore, the explosible character of AlSi10Mg creates a safety risk during handling for operators, implying high safety equipment costs often accompanied by investments in the manufacturing environment [6]. Innovative AlSi10Mg formulations with non-explosible features can lower and even eliminate risks during the L-PBF process, drastically decreasing operational cost. Moreover, the cost of NExP-1 powder is set to approximately 85 USD/kg, while prices for standard AlSi10Mg feedstock of 30-60 µm particle diameters from North American suppliers can range between 135-145 USD/kg.

Commercially available AlSi10Mg powder typically ranges between 20-70 µm for medium-wattage industrial L-PBF machines, for both spherical and elliptic granules [5]. Spherically shaped particles with uniform distribution at higher diameters enable superior build rates due to increased flowability coupled with the option of printing at higher layer thicknesses [7]. Thicker powder causes atypical energy penetration in the melt pool [8], necessitating L-PBF process parameter optimization towards achieving adequate part density and strength. The NExP-1 non-explosible powder from Equispheres, standing out among commercial equivalents, is homogenously spherical-shaped with a power size distribution above 100 µm; these characteristics can potentially meet the aforementioned high built rate requirements in an affordable manufacturing environment. Literature [9] suggests that parts fabricated with NExP-1 can display close to full density and good mechanical

properties on 700 W (high-wattage) L-PBF machines. However, additive manufacturing and part characterization with this innovative powder on medium-wattage (400 W) equipment is not yet researched.

This study aims to characterize NexP-1 powder explosiveness and to develop the processing of highly homogenous spherical AlSi10Mg of over 100 µm particle size distribution in an affordable L-PBF machine with a 400 W Yb-fiber laser. The non-explosible claim of the NExP-1 AlSi10Mg powder was analyzed through Lower Explosive Limit (LEL) per JIS Z 8818, Minimum Ignition Energy (MIE) per JIS Z 8834 and Explosion Class per JIS Z 8817. Density and mechanical test characterizations were performed on 3D printed AlSi10Mg parts towards L-PBF process parameter optimization.

Material and Methods

The study unfolds over two steps, beginning with the explosibility characterizations of NExP-1 AlSi10Mg powder (Equispheres, Canada) followed by L-PBF process parameter optimization. The chemical composition of NExP-1 powder is included in Table 1. An SEM image of the uniform and spherical powder was exhibited in Figure 1.a, while the powder size approaches and even exceeds 100 µm as illustrated by the cumulative size distribution graph in Figure 1.b.

Table 1. Chemical Composition of AlSi10Mg-NExP-1powder in wt.%

Al	Si	Mg	Fe	Ti	Mn	Cu	Zn
Base	9.0-11-0	0.20-0.45	0.20	0.10	0.10	0.05	0.10

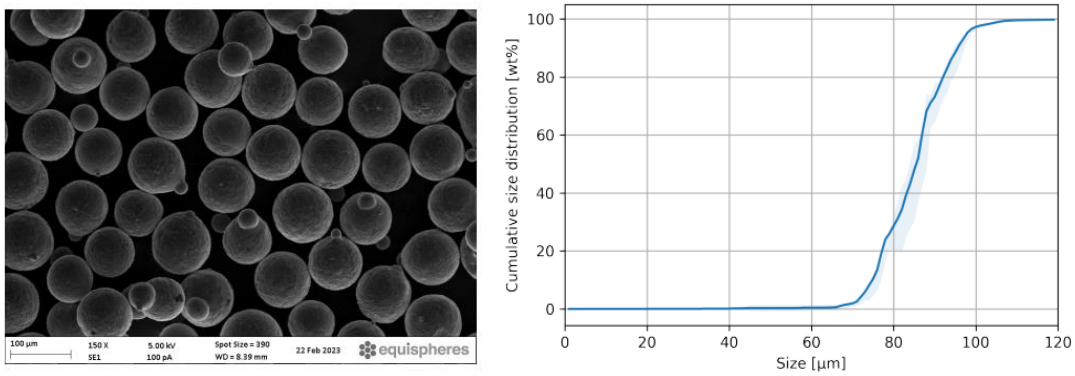

(a) (b)

Figure 1. (a) NExP-1 AlSi10Mg powder SEM image. (b) Cumulative powder size distribution of NExP-1 [9].

The explosibility of NExP-1 was evaluated under the Lower Explosive Limit (LEL) according to JIS Z 8818 (⇔ASTM E 1515-07) and Minimum Ignition Energy (MIE) according to JIS Z 8834 (⇔ISO/IEC 61241-2-3). Two separate aluminum powders, which are Powder A-AlSi10Mg and Powder B-Pure Al powder, were produced using the gas atomization technique and assessed along with NExP-1 powder under the same conditions. The explosion class of NExP-1 powder was determined by Maximum Explosion Pressure (MEP) analysis according to JIS Z 8817 (⇔ASTM E 1226). The Hartmann-type test apparatus (Figure 2.a) was used to measure the propagation of flame height using a Hartmann-type blow-off for LEL and MIE characterizations. An explosion spherical container (Figure 2.b) was utilized to measure explosion pressure in LEL and MEP.

(a) (b)

Figure 2. (a) Hartmann-type test apparatus, (b) Explosion spherical container.

Concerning process parameter optimization, sixteen different parameter sets were proposed, with one solid cube of side equal to 12 mm manufactured per set on a medium-wattage L-PBF machine (XM200G, Xact Metal, USA) (Table 2). A stripe scanning strategy was adopted and border parameters were disabled. The main parameters are a constant 390 W laser power (P), close to the maximum 400 W of the machine and a constant 60 μm layer thickness (t) due to manufacturer recommendations as per the NExP-1 datasheet [9]. The rationale is that the effective layer thickness, which is a function of packing density and approximately equals double the vertical build plate displacement after seven coating passes [7] should exceed the D90 particle size distribution. Given the latter's value of 99 μm and the calculated effective layer thickness of 60 μm layers to be approximately 110 μm, this condition is met.

The scanning speed (v) range was between 750-1250 mm/s while the hatch distance (s) varied between 0.09 and 0.19 μm. The combination of these parameters was defined as the volumetric energy density, VED, of Equation 1 [10], characterizing the energy within the melt pool.

$$VED = \frac{P}{v.t.s} \qquad (1)$$

Table 2. Parameter sets for L-PBF process parameter optimization.

Scanning Speed (mm/s)	Hatch Distance (mm)	Volumetric Energy Density (J/mm^3)
1250	0.09	57.77
	0.11	47.27
	0.13	40
	0.16	32.50
	0.19	27.36
1100	0.09	65.65
	0.11	53.71
	0.13	45.45
900	0.13	55.55
	0.15	48.14
	0.17	42.48
	0.19	38.01
750	0.13	66.66
	0.15	57.77
	0.17	50.98
	0.19	45.61

Density characterizations were subsequently performed using metallographic analysis after manufacturing all parameter sets. The specimens were cut parallel to the building direction, then ground and polished on a post-processing unit (QATM, Germany) to obtain mirror surfaces that would reveal any manufacturing imperfections. These defects were imaged via a light optical microscope (LOM) (Keyence, Japan).

Two parameter sets, 1250 mm/s-0.11 mm and 1100 mm/s-0.13 mm, displaying the highest density, were used to manufacture three horizontally oriented tensile samples per set. These were subsequently tested at a displacement rate of 5 mm/min on a tensile tester (Z010 10kN, Zwick Roell, Germany) equipped with a mechanical extensometer (Digiclip, Zwick Roell, Germany) according to ASTM E8. Fracture surface images were acquired using a scanning electron microscope (SEM) (Hitachi S-4800, Japan). Surface roughness was measured on the 1100 mm/s-0.13 mm parameter samples employing a surface profilometer (Dektak, Brukel).

Results and Discussions

Explosion Results and Discussions

Regarding the LEL of Figure 3, Powder A exhibited 39 mJ, with Powder B proving even more dangerous, at below 10 mJ. The LEL of NExP-1 is significantly higher, indicating superior safety. NExP-1 powder showed that no explosion occurred even at the test upper limit energy of 300 mJ. Based on these results, it can be concluded that NExP-1 powder can significantly reduce the risk of dust explosions at actual manufacturing sites, lowering the setup cost.

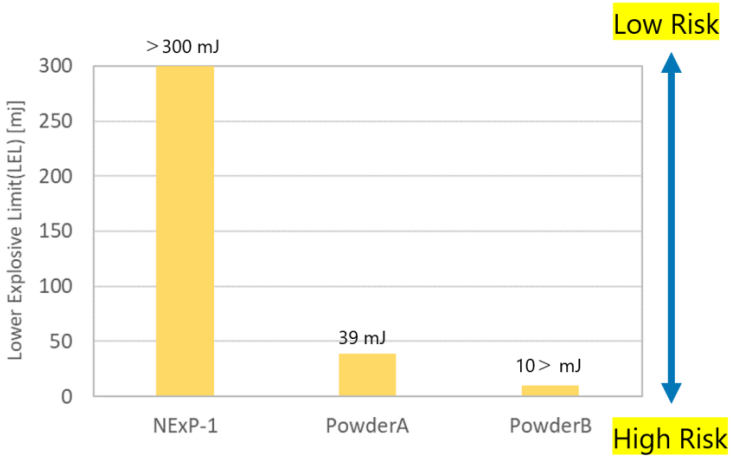

Figure 3. Lower Explosive Limit (LEL) graph of three different powders: NExP-1, Powder A (AlSi10Mg) and Powder B (Pure Al).

MIE values were measured to be 190 g/m^3 for Powder A and 30 g/m^3 for Powder B, while the 440 g/m^3 for NExP-1 powder was more than twice that of Powder A (Figure 4.a). The explosibility of NExP-1 is overwhelmingly low in the MIE test as well as in the LEL test. NExP-1's explosion possibility based on the JIS standard was classified as the lowest level of danger. Figure 4.b shows that the explosive intensity of NExP-1 powder was drastically reduced compared to Powder A and Powder B. A dust explosion occurred due to the combustion of the dust cloud, which caused rapid volumetric expansion under JIS-Z-8812. The ignition of Powder B, which gave the lowest MIE energy value, was observed at 200 g/m^3 from the first seconds, while the explosion stopped at 15 seconds in a Hartmann-type test apparatus. The ignition of Powder A at 600 g/m^3 occurred after 12 seconds, with the explosion stopping 24 seconds later. NExP-1 powder, which had an MIE value of 440 g/m^3, was ignited at 1000 g/m^3 from the 18th second, with a less aggressive combustion observed in the 30th second.

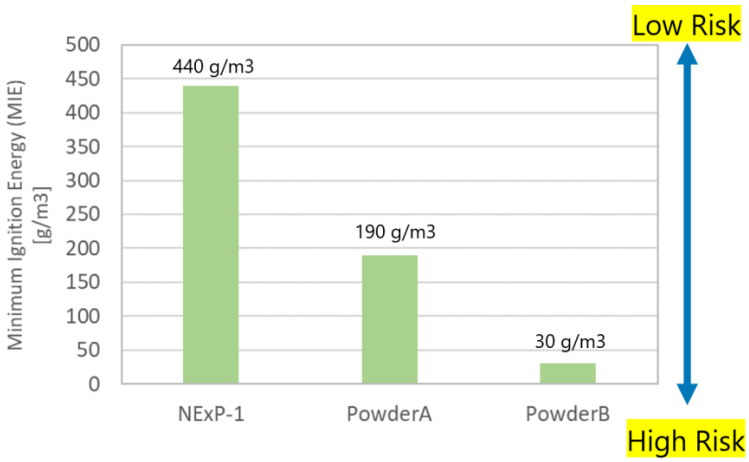

(a)

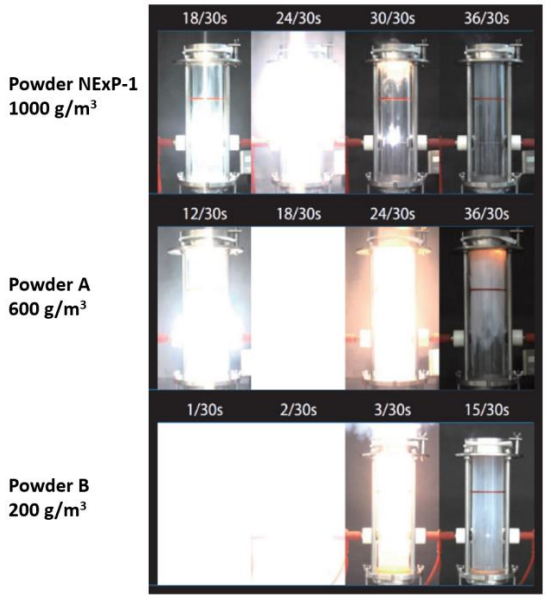

(b)

Figure 4. (a) Minimum Ignition Energy (MIE) of the graph of three different powders. NExP-1, Powder A (AlSi10Mg) and Powder B (Pure Al). (b) Progress of dust explosion tests based on JIS-Z-8812

A big difference was shown in the intensity of explosion among powders; Powder A had $6x10^2$ kPa while Powder B had $11.5x10^2$ kPa (Figure 5). No pressure rise in NExP-1 powder was observed in the explosion container during the test. As a result, NExP-1 powder was classified as st0, certifying its non-explosive nature.

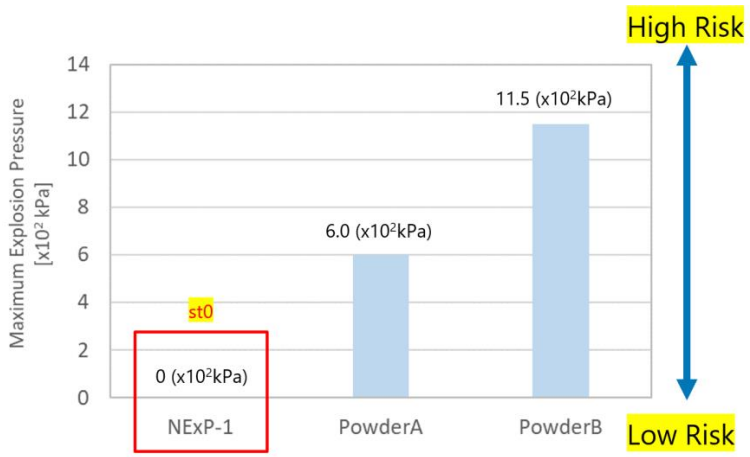

Figure 5. Maximum Explosion Pressure graph of three different powders. NExP-1, Powder A (AlSi10Mg) and Powder B (Pure Al).

Density Characterization Results and Discussions

Figure 6 shows mirror surface images per parameter set in a scanning speed-hatch distance graph under constant 390 W laser power and 60 µm layer thickness. Reduction in defect formation was observed at 750 and 900 mm/s scanning speeds as the hatch distance was increased from 0.13 to 0.19 mm. The reason for the defect reduction might relate to high volumetric energy density, in other means penetrated energy to the melt pool caused keyhole porosity formation [11]. Increasing hatch distance greatly grew manufacturing quality at low scanning speeds, while increasing scanning speed adversely influenced the quality at the same hatch distance range. An increase in surface defects was seen in increasing the hatch distance from 0.17 to 0.19 mm at a speed of 1250 mm/s. Increasing hatch distance reduces the penetrated energy towards the melt pool, resulting in the lack of fusion porosity [10]. On the other hand, the lowest defect formation was observed at 1250 mm/s-0.11 mm and 1100 mm/s-0.13 mm parameter combinations. VED values of these parameter sets were calculated as 45 and 47 J/mm^3, seen as quite close values to each other.

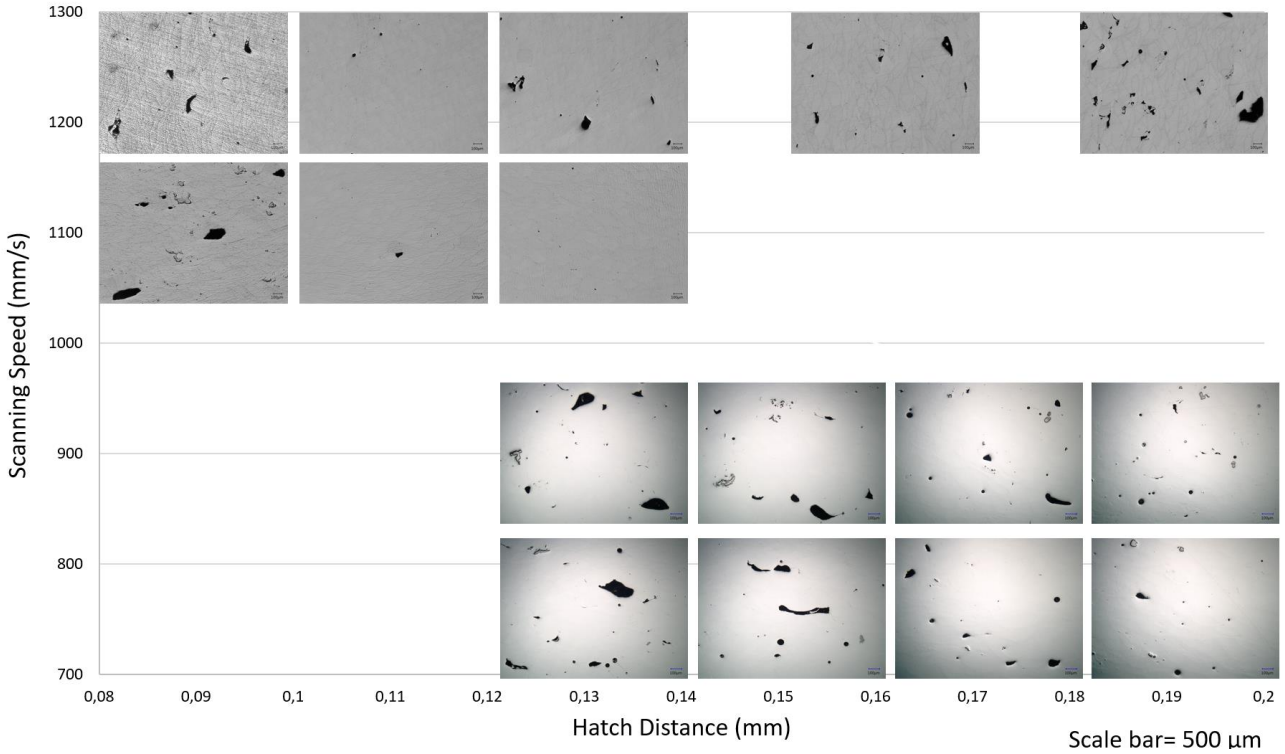

Figure 6. Scanning Speed-Hatch Distance graph of 16 different parameter sets for L-PBF process parameter optimization.

Mechanical Test Results and Discussions

Tensile tests were performed on samples from the two parameter sets which displayed the lowest defect formations as shown in Figure 7. Table 3 highlights the ultimate tensile strength (UTS) and yield strength (YS) of 1250 mm/s-0.11 mm samples at 316 MPa and 185 MPa, respectively; a 3.6% elongation value was measured. The 1100 mm/s-0.13 mm samples exhibited higher mechanical performance (355 MPa UTS, 220 MPa YS) and 4.4% elongation, attributed to lower defect distribution. The results of both parameters, especially the 1100 mm/s-0.13 mm parameter are compatible with the literature [12,13] despite intra-part manufacturing defects. Paul et al., 2021 [14] reached a 98% Archimedes density rate, along with 189-213 MPa in YS and 323-340 MPa as UTS at 60 µm layer thickness. The one exception is linked to the 6.7% elongation value that exceeds that of the 1100 mm/s-0.13 mm samples. On the other hand, the results of Aboulkhair et al. and Read et al. for horizontal dog bone tensile tests [15,16] are in line with the UTS and YS outcomes of this study whereas their elongation values are lower than those measured for the two characterized sample sets. The study [15] explained that the reason for lower elongation is associated with poorer surface roughness values. The measured surface roughness was 3.85±1.5 µm for this study. Thus, Praneeth et al. revealed 3.53 µm surface roughness and similar tensile test results to this study's values [17].

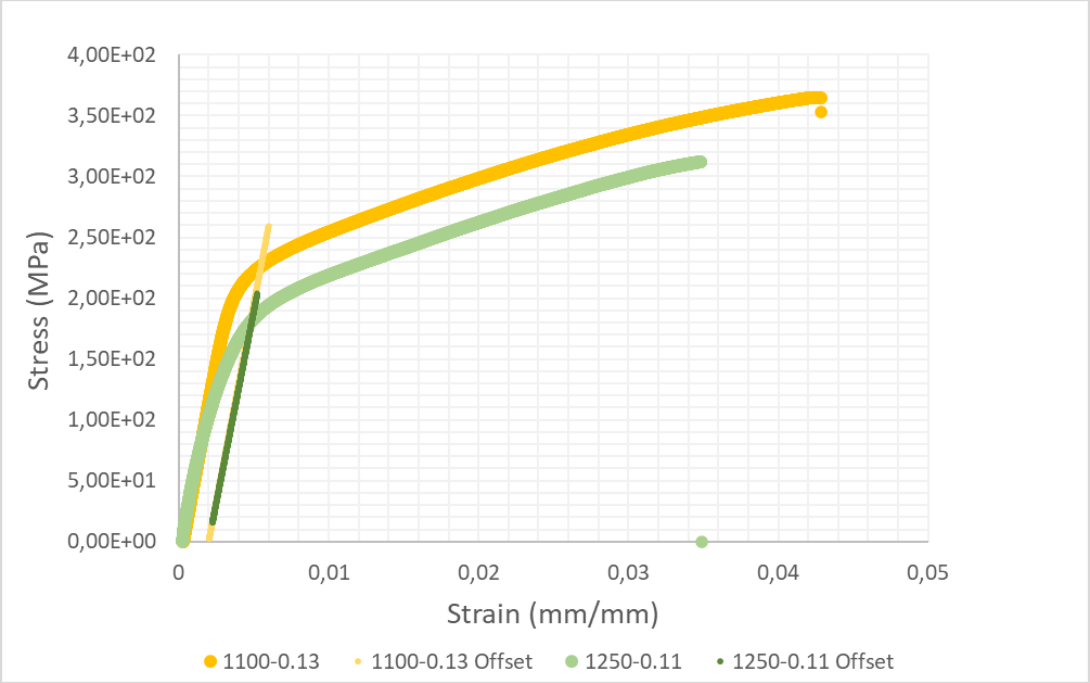

Figure 7. Stress-strain graph of tensile tested dog bones manufactured with 1250 mm/s-0.11 mm and 1100 mm/s-0.13 mm parameter sets.

Table 3. Mechanical properties of tensile-tested dog bones manufactured by two parameter sets

Parameters	UTS (MPa)	YS (MPa)	Elongation (%)
390 W, 1250 mm/s, 0.06 mm, 0.11 mm	316.3±4.5	185.3±5.8	3.6±0.2
390 W, 1100 mm/s, 0.06 mm, 0.13 mm	355.3±13.6	220±4	4.4±0.3

Figure 8.a and b exhibited the SEM images of tensile-tested dog bone fracture surfaces for both the 1250 mm/s-0.11 mm and 1100 mm/s-0.13 mm sets. Brittle fractures with no dimple-like features were observed for both parameters. More than one layers were shown at the fracture surface in Figure 8.a regarding the layer-by-layer L-PBF principle. The reason for the fracture might be the defect formations illustrated in Figure 6. Figure 8.c also shows shear rupture at the horizontal-orientated flat tensile specimen manufactured with 1100 mm/s-0.13 mm. Paul et al. 2021 [14] explained that shear fracture is linked to the lack of tri-axiality since horizontal dog bones were tested perpendicular to the building rate.

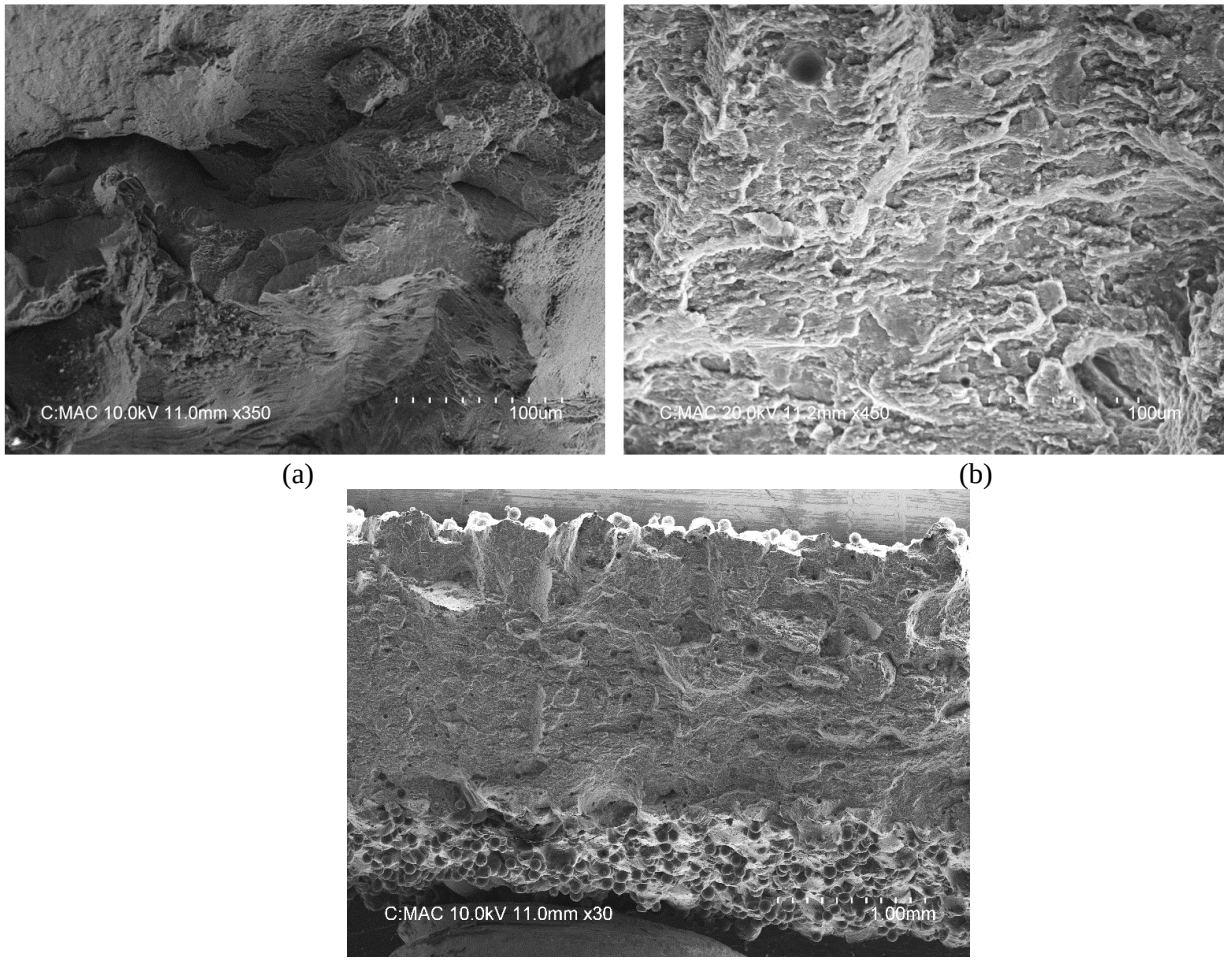

(a) (b)

(c)

Figure 8. SEM images of tensile-tested dog bones fracture surface (a) 1250 mm/s-0.11 mm, (b) 1100 mm/s-0.13 mm, (c) 1100 mm/s-0.13 mm.

Conclusion

The explosibility results classify NExP-1 as an outstandingly safe feedstock for L-PBF, rendering it very attractive in a manufacturing setup for lightweight applications. The UTS and YS values of NExP-1 AlSi10Mg align with the literature despite defect formation. This innovative powder, however, is still open to development for medium-wattage machines towards achieving almost full density. 1100 mm/s-0.13 mm hatch distance with constant 390 W and 0.06 mm layer thickness has been linked to the lowest defect formation and the highest mechanical strength. Having reached the maximum recommended laser power, as the machine's limitation, can encourage different scanning strategies and post-processing techniques to be applied for thick powder over 100-micron powder size. Consequently, this study shows the promising future of non-explosible aluminum-alloy powder for the adoption of affordable additive manufacturing, at no cost to part density or mechanical performance.

Acknowledgement

We would like to acknowledge Evan Butler-Jones and José Muñiz from Equispheres for their openness towards discussions and fruitful dialogue on process parameter considerations.

References

[1] J. A. T. Rios, P. Zambrano-Robledo, J. D. T. Taborda, J. A. G. Espinoza, C. J. Isaza, and A. Juárez-Hernández, "Process parameters effect and porosity reduction on AlSi10Mg parts manufactured by selective laser melting," *The International Journal of Advanced Manufacturing Technology 2023 129:7*, vol. 129, no. 7, pp. 3341–3351, Oct. 2023, doi: 10.1007/S00170-023-12521-8.

[2] Z. Li, B. Q. Li, P. Bai, B. Liu, and Y. Wang, "Research on the Thermal Behaviour of a Selectively Laser Melted Aluminium Alloy: Simulation and Experiment," *Materials 2018, Vol. 11, Page 1172*, vol. 11, no. 7, p. 1172, Jul. 2018, doi: 10.3390/MA11071172.

[3] M. A. Balbaa, A. Ghasemi, E. Fereiduni, M. A. Elbestawi, S. D. Jadhav, and J. P. Kruth, "Role of powder particle size on laser powder bed fusion processability of AlSi10mg alloy," *Addit Manuf*, vol. 37, p. 101630, Jan. 2021, doi: 10.1016/J.ADDMA.2020.101630.

[4] S. Czink, V. Schulze, and S. Dietrich, "EXPERIMENTAL INVESTIGATIONS OF INHOMOGENEOUS COMPONENT PROPERTIES IN LASER-BASED ADDITIVE MANUFACTURING OF AlSi10Mg".

[5] P. Yang *et al.*, "Effect of thermal annealing on microstructure evolution and mechanical behavior of an additive manufactured AlSi10Mg part," *J Mater Res*, vol. 33, no. 12, pp. 1701–1712, Jun. 2018, doi: 10.1557/JMR.2018.82/FIGURES/8.

[6] A. Raja, S. R. Cheethirala, P. Gupta, N. J. Vasa, and R. Jayaganthan, "A review on the fatigue behaviour of AlSi10Mg alloy fabricated using laser powder bed fusion technique," *Journal of Materials Research and Technology*, vol. 17, pp. 1013–1029, Mar. 2022, doi: 10.1016/J.JMRT.2022.01.028.

[7] H. W. Mindt, M. Megahed, N. P. Lavery, M. A. Holmes, and S. G. R. Brown, "Powder Bed Layer Characteristics: The Overseen First-Order Process Input," *Metall Mater Trans A Phys Metall Mater Sci*, vol. 47, no. 8, pp. 3811–3822, Aug. 2016, doi: 10.1007/S11661-016-3470-2/METRICS.

[8] U. Scipioni Bertoli, A. J. Wolfer, M. J. Matthews, J. P. R. Delplanque, and J. M. Schoenung, "On the limitations of Volumetric Energy Density as a design parameter for Selective Laser Melting," *Mater Des*, vol. 113, pp. 331–340, Jan. 2017, doi: 10.1016/j.matdes.2016.10.037.

[9] Equispheres Inc., "Chemical Composition * Per ASTM B213-20 ** Per ASTM B964-16," 2022. Accessed: Jun. 24, 2024. [Online]. Available: https://equispheres.com/material-data-sheet-nexp-1-alsi10mg/

[10] F. N. Depboylu, E. Yasa, O. Poyraz, and F. Korkusuz, "Thin-Walled Commercially Pure Titanium Structures: Laser Powder Bed Fusion Process Parameter Optimization," *Machines 2023, Vol. 11, Page 272*, vol. 11, no. 2, p. 272, Feb. 2023, doi: 10.3390/MACHINES11020272.

[11] N. T. Aboulkhair, M. Simonelli, L. Parry, I. Ashcroft, C. Tuck, and R. Hague, "3D printing of Aluminium alloys: Additive Manufacturing of Aluminium alloys using selective laser melting," *Prog Mater Sci*, vol. 106, p. 100578, Dec. 2019, doi: 10.1016/J.PMATSCI.2019.100578.

[12] Z. H. Xiong, S. L. Liu, S. F. Li, Y. Shi, Y. F. Yang, and R. D. K. Misra, "Role of melt pool boundary condition in determining the mechanical properties of selective laser melting AlSi10Mg alloy," *Materials Science and Engineering: A*, vol. 740–741, pp. 148–156, Jan. 2019, doi: 10.1016/J.MSEA.2018.10.083.

[13] E. W. Hovig, A. S. Azar, M. Mhamdi, and K. Sørby, "Mechanical Properties of AlSi10Mg Processed by Laser Powder Bed Fusion at Elevated Temperature," *Minerals, Metals and Materials Series*, pp. 395–404, 2020, doi: 10.1007/978-3-030-36296-6_37.

[14] M. J. Paul *et al.*, "Fracture resistance of AlSi10Mg fabricated by laser powder bed fusion," *Acta Mater*, vol. 211, p. 116869, Jun. 2021, doi: 10.1016/J.ACTAMAT.2021.116869.

[15] N. T. Aboulkhair, I. Maskery, C. Tuck, I. Ashcroft, and N. M. Everitt, "The microstructure and mechanical properties of selectively laser melted AlSi10Mg: The effect of a conventional T6-like heat treatment," *Materials Science and Engineering: A*, vol. 667, pp. 139–146, Jun. 2016, doi: 10.1016/J.MSEA.2016.04.092.

[16] N. Read, W. Wang, K. Essa, and M. M. Attallah, "Selective laser melting of AlSi10Mg alloy: Process optimisation and mechanical properties development," *Materials & Design (1980-2015)*, vol. 65, pp. 417–424, Jan. 2015, doi: 10.1016/J.MATDES.2014.09.044.

[17] J. Praneeth, S. Venkatesh, and L. S. Krishn, “Process parameters influence on mechanical properties of AlSi10Mg by SLM,” *Mater Today Proc*, Jan. 2023, doi: 10.1016/J.MATPR.2022.12.222.